SLAC-PUB-11615, UFIFT-HEP-06-02, UCRL-JRNL-220485

Hadron Optics: Diffraction Patterns in Deeply Virtual Compton Scattering

S. J. Brodsky[a], **D. Chakrabarti**[b], **A. Harindranath**[c], **A. Mukherjee**[d], **J. P. Vary**[e,a,f]

[a] *Stanford Linear Accelerator Center, Stanford University, Stanford, California 94309, USA.*

[b] *Department of Physics, University of Florida, Gainesville, FL-32611-8440, USA.*

[c] *Saha Institute of Nuclear Physics, 1/AF Bidhannagar, Kolkata 700064, India.*

[d] *Department of Physics, Indian Institute of Technology, Powai, Mumbai 400076, India.*

[e] *Department of Physics and Astronomy, Iowa State University, Ames, Iowa 50011, USA.*

[f] *Lawrence Livermore National Laboratory, L-414, 7000 East Avenue, Livermore, California, 94551, USA.*

(Dated: 27 April, 2006)

Abstract

We show that the Fourier transform of the Deeply Virtual Compton Scattering (DVCS) amplitude with respect to the skewness variable ζ provides a unique way to visualize the light-front wavefunctions (LFWFs) of the target state in the boost-invariant longitudinal coordinate space variable ($\sigma = \frac{P^+ y^-}{2}$). The results are analogous to the diffractive scattering of a wave in optics in which the dependence of the amplitude on σ measures the physical size of the scattering center of a one-dimensional system. If one combines this longitudinal transform with the Fourier transform of the DVCS amplitude with respect to the transverse momentum transfer $\Delta^\perp$, one can obtain a complete three-dimensional description of hadron optics at fixed light-front time $\tau = t + z/c$. As a specific example, we utilize the quantum fluctuations of a fermion state at one loop in QED to obtain the behavior of the DVCS amplitude for electron-photon scattering. We then simulate the wavefunctions for a hadron by differentiating the above LFWFs with respect to M^2 and study the corresponding DVCS amplitudes in σ space.

Submitted to Physical Review D

Work supported in part by Department of Energy contract DE-AC02-76SF00515

Introduction

Deeply virtual Compton scattering $\gamma^*(q)p \to \gamma(k)p'$ provides a remarkable tool for studying the fundamental structure of the proton at the amplitude level. When the incoming photon is highly virtual $Q^2 = -q^2 >> \Lambda^2_{QCD}$, the underlying scattering process measures Compton scattering on bound quarks, convoluted with the fundamental microscopic wavefunctions of the initial- and final-state proton. In addition, the initial-state photon can scatter on virtual $q\bar{q}$ pairs in the target which are then annihilated by the final-state photon, thus probing the particle-number quantum fluctuations of the hadron wavefunction required for Lorentz invariance. Measurements of the DVCS cross sections with specific proton and photon polarizations can provide comprehensive probes of the spin as well as spatial structure of the proton at the most fundamental level of QCD.

The theoretical analysis of DVCS is particularly clear and compelling when one utilizes light-front quantization at fixed $\tau = y^+ = t + z/c$. If we neglect radiative corrections to the struck quark propagator (i.e., set the Wilson line to 1), then the required DVCS quark matrix elements can be computed from the overlap of the boost-invariant light-front Fock state wavefunctions of the target hadron [1, 2]. The longitudinal momentum transfer to the target hadron is given by the "skewness" variable $\zeta = \frac{Q^2}{2p\cdot q}$. Since the incoming photon is spacelike ($q^2 < 0$) and the final photon is on-shell ($k^2 = 0$), the skewness is never zero in a physical experiment. The DVCS process involves off-forward hadronic matrix elements of light-front bilocal currents; accordingly, there is a diagonal parton-number conserving $n \to n$ overlap in the kinematical regime $\zeta < x < 1$ and $\zeta - 1 < x < 0$ and an off-diagonal $n+1 \to n-1$ overlap for $0 < x < \zeta$, where the parton number is decreased by two. Thus, given the LFWFs one then obtains a complete specification of all of the generalized parton distributions measurable in DVCS, including their phase structure. The sum rules of DVCS, such as Ji's sum rule for angular momentum [3] and the integral relations to electromagnetic and gravitational form factors are all explicitly satisfied in the LF formalism [1, 2].

In this paper we shall show how one can use measurements of the dependence of the DVCS amplitude on the skewness variable ζ to obtain a novel optical image of a hadron target, in analogy to the way in which one scatters optical waves to form a diffraction pattern. The Fourier transform of the DVCS amplitude with respect to ζ allows one to determine the longitudinal structure of the target hadron in terms of the variable $\sigma = \frac{1}{2}y^- P^+$, the boost-

invariant longitudinal spatial coordinate conjugate to the light-front longitudinal momentum variable, ζ. (We use the standard LF coordinates $P^{\pm} = P^0 \pm P^3, y^{\pm} = y^0 \pm y^3$. Since the proton is on-shell, $P^+P^- - P_\perp^2 = M_p^2$). If one combines this longitudinal transform with the Fourier transform of the DVCS amplitude with respect to the transverse momentum transfer $\Delta^\perp$ [4, 5], one can obtain a complete three-dimensional description of hadron optics at fixed LF time.

In principle, the LFWFs of hadrons in QCD can be computed using a nonperturbative method such as Discretized Light Cone Quantization (DLCQ) where the LF Hamiltonian is diagonalized on a free Fock basis [6]. This has been accomplished for simpler confining quantum field theories such as $QCD(1+1)$ [7]. Models for the LFWFs of hadrons in $(3+1)$ dimensions displaying confinement at large distances and conformal symmetry at short distances have been obtained using the AdS/CFT method [8]. The y^- structure of topological objects has been studied in [9] in DLCQ.

In order to illustrate our general framework, we will present here an explicit calculation of the σ transform of virtual Compton scattering on the quantum fluctuations of a lepton in QED at one-loop order [10], the same system which gives the Schwinger anomalous moment $\alpha/2\pi$. One can generalize this analysis by assigning a mass M to the external electrons and a different mass m to the internal electron lines and a mass λ to the internal photon lines with $M < m + \lambda$ for stability. In effect, we shall represent a spin-$\frac{1}{2}$ system as a composite of a spin-$\frac{1}{2}$ fermion and a spin-1 vector boson [11–13]. We also will present numerical results for a composite hadron by taking a derivative of the LFWFs with respect to the hadron's mass M^2. This simulates the behavior of a bound-state hadron by improving the fall-off the end points of x. The summary of our main results will be given in this letter. A more detailed analysis will be given in a forthcoming article [14].

DVCS in the LF Formalism

The kinematics of the DVCS process has been given in detail in [1, 2]. One can work in a frame where the momenta of the initial and final proton has a $\Delta \to -\Delta$ symmetry [2]; with $\Delta = P - P'$ and $t = \Delta^\mu \Delta_\mu$. However, in this frame, the kinematics in terms of the parton momenta becomes more complicated. Here, we shall use the frame choice of Ref. [1].

The virtual Compton amplitude $M^{\mu\nu}(\vec{q}_\perp, \vec{\Delta}_\perp, \zeta)$, *i.e.*, the transition matrix element of the process $\gamma^*(q) + p(P) \to \gamma(q') + p(P')$, can be defined from the light-cone time-ordered

product of currents

$$M^{\mu\nu}(\vec{q}_\perp, \vec{\Delta}_\perp, \zeta) \;=\; i \int d^4y\, e^{-iq\cdot y} \langle P'|T J^\mu(y) J^\nu(0)|P\rangle \;, \tag{1}$$

where the Lorentz indices μ and ν denote the polarizations of the initial and final photons respectively. In the limit $Q^2 \to \infty$ at fixed ζ and t the Compton amplitude is thus given by

$$\begin{aligned} M^{IJ}(\vec{q}_\perp, \vec{\Delta}_\perp, \zeta) \;&=\; \epsilon^I_\mu\, \epsilon^{*J}_\nu\, M^{\mu\nu}(\vec{q}_\perp, \vec{\Delta}_\perp, \zeta) \;=\; -e_q^2\, \frac{1}{2\bar{P}^+} \int_{\zeta-1}^{1} \mathrm{d}x \\ &\times \left\{ t^{IJ}(x,\zeta)\, \bar{U}(P') \left[H(x,\zeta,t)\, \gamma^+ + E(x,\zeta,t)\, \frac{i}{2M}\, \sigma^{+\alpha}(-\Delta_\alpha) \right] U(P) \right\}, \end{aligned} \tag{2}$$

where $\bar{P} = \frac{1}{2}(P' + P)$ and we take a frame in which $q^+ = 0$. For DVCS, when Q^2 is large compared to the masses and $-t$, we have,

$$\frac{Q^2}{2P\cdot q} = \zeta \tag{3}$$

up to corrections in $1/Q^2$. Thus ζ plays the role of the Bjorken variable in deeply virtual Compton scattering. For a fixed value of $-t$, the allowed range of ζ is given by

$$0 \;\le\; \zeta \;\le\; \frac{(-t)}{2M^2} \quad \left(\sqrt{1 + \frac{4M^2}{(-t)}} \;-\; 1 \right) \;. \tag{4}$$

For simplicity we only consider one quark with flavor q and electric charge e_q. We here consider the contribution of only the spin-independent GPDs H and E. Throughout our analysis we will use the "handbag" approximation where corrections to the hard quark propagator are neglected.

For circularly polarized initial and final photons ($I,\ J$ are $\uparrow$ or $\downarrow$)) contributions only come from

$$t^{\,\uparrow\uparrow}(x,\zeta) \;=\; \quad t^{\,\downarrow\downarrow}(x,\zeta) \;=\; \frac{1}{x - i\epsilon} \;+\; \frac{1}{x - \zeta + i\epsilon} \;. \tag{5}$$

For a longitudinally polarized initial photon, the Compton amplitude is of order $1/Q$ and thus vanishes in the limit $Q^2 \to \infty$. At order $1/Q$ there are several corrections to the simple structure in Eq. (2). We do not consider them here.

The generalized parton distributions H, E are defined through matrix elements of the bilinear vector and axial vector currents on the light-cone:

$$\begin{aligned} F_{\lambda,\lambda'} &= \int \frac{dy^-}{8\pi}\, e^{ixP^+y^-/2}\, \langle P', \lambda'|\bar{\psi}(0)\, \gamma^+\, \psi(y)\, |P, \lambda\rangle \Big|_{y^+=0, y_\perp=0} \\ &=\; \frac{1}{2\bar{P}^+}\, \bar{U}(P', \lambda') \left[H(x,\zeta,t)\, \gamma^+ + E(x,\zeta,t)\, \frac{i}{2M}\, \sigma^{+\alpha}(-\Delta_\alpha) \right] U(P, \lambda) \;, \end{aligned} \tag{6}$$

The off-forward matrix elements given by Eq. (6) can be expressed in terms of overlaps of LFWFs of the state [1, 2]. For this, we take the state to be an electron in QED at one loop and consider the LFWFs for this system.

The light-front Fock state wavefunctions corresponding to the quantum fluctuations of a physical electron can be systematically evaluated in QED perturbation theory. The state is expanded in Fock space and there are contributions from $|\, e^-\gamma\rangle$ and $|\, e^-e^-e^+\rangle$, in addition to renormalizing the one-electron state. The two-particle state is expanded as,

$$\begin{aligned}\left|\Psi^{\uparrow}_{\text{two particle}}(P^+,\vec{P}_\perp=\vec{0}_\perp)\right\rangle = \int \frac{\mathrm{d}x\,\mathrm{d}^2\vec{k}_\perp}{\sqrt{x(1-x)}\,16\pi^3} \\ \Big[\;\; \psi^{\uparrow}_{+\frac{1}{2}+1}(x,\vec{k}_\perp)\left|+\frac{1}{2}+1\,;\; xP^+\,,\;\vec{k}_\perp\right\rangle + \psi^{\uparrow}_{+\frac{1}{2}-1}(x,\vec{k}_\perp)\left|+\frac{1}{2}-1\,;\; xP^+\,,\;\vec{k}_\perp\right\rangle \\ + \psi^{\uparrow}_{-\frac{1}{2}+1}(x,\vec{k}_\perp)\left|-\frac{1}{2}+1\,;\; xP^+\,,\;\vec{k}_\perp\right\rangle + \psi^{\uparrow}_{-\frac{1}{2}-1}(x,\vec{k}_\perp)\left|-\frac{1}{2}-1\,;\; xP^+\,,\;\vec{k}_\perp\right\rangle\Big]\;,\end{aligned} \tag{7}$$

where the two-particle states $|s^z_{\rm f}, s^z_{\rm b};\; x, \vec{k}_\perp\rangle$ are normalized as in [1]. The variables $s^z_{\rm f}$ and $s^z_{\rm b}$ denote the projection of the spins of the constituent fermion and boson along the quantization axis, and the variables x and $\vec{k}_\perp$ refer to the momentum of the fermion. The light cone momentum fractions $x_i = \frac{k_i^+}{P^+}$ satisfy $0 < x_i \leq 1$, $\sum_i x_i = 1$. We employ the light-cone gauge $A^+ = 0$, so that the gauge boson polarizations are physical. The three-particle state has a similar expansion. Both the two- and three-particle Fock state components are given in [1]. We list here the two-particle wavefunctions for the spin-up electron [1, 10, 15]

$$\begin{cases} \psi^{\uparrow}_{+\frac{1}{2}+1}(x,\vec{k}_\perp) = -\sqrt{2}\;\frac{-k^1+ik^2}{x(1-x)}\,\varphi\;, \\ \psi^{\uparrow}_{+\frac{1}{2}-1}(x,\vec{k}_\perp) = -\sqrt{2}\;\frac{k^1+ik^2}{1-x}\,\varphi\;, \\ \psi^{\uparrow}_{-\frac{1}{2}+1}(x,\vec{k}_\perp) = -\sqrt{2}\;(M-\frac{m}{x})\,\varphi\;, \\ \psi^{\uparrow}_{-\frac{1}{2}-1}(x,\vec{k}_\perp) = 0\;, \end{cases} \tag{8}$$

$$\varphi(x,\vec{k}_\perp) = \frac{e}{\sqrt{1-x}}\;\frac{1}{M^2-\frac{\vec{k}_\perp^2+m^2}{x}-\frac{\vec{k}_\perp^2+\lambda^2}{1-x}}\;. \tag{9}$$

Similarly, the wavefunction for an electron with negative helicity can also be obtained.

At $x = 1$, there are contributions from the overlap of one particle states which depend on the wavefunction renormalization constant Z. We have imposed a cutoff on x near this point. Also, in order to regulate the ultraviolet divergences, we use a cutoff Λ on the transverse momentum $k^\perp$.

In the domain $\zeta < x < 1$, there are diagonal $2 \to 2$ overlap contributions to Eq. (6), both helicity flip, F^{22}_{+-} ($\lambda' \neq \lambda$) and helicity non-flip, F^{22}_{++} ($\lambda' = \lambda$) [1]. The GPDs $H_{(2\to 2)}(x,\zeta,t)$

and $E_{(2\to 2)}(x,\zeta,t)$ are zero in the domain $\zeta - 1 < x < 0$, which corresponds to emission and reabsorption of an e^+ from a physical electron. Contributions to $H_{(n\to n)}(x,\zeta,t)$ and $E_{(n\to n)}(x,\zeta,t)$ in that domain only appear beyond one-loop level.

The matrix elements F^{22}_{++} and F^{22}_{+-} are calculated using the two-particle LFWFs given in Eq. (8). The contributions in the domain, $0 < x < \zeta$, namely, F^{31}_{+-} and F^{31}_{++} come from overlaps of three-particle and one-particle LFWFs [1]. Z is taken to be 1 here. These are calculated using the three-particle wavefunction. Explicit expressions of all the above matrix elements will be given in [14].

We calculate the DVCS amplitude given by Eq. (2) using the off-forward matrix elements calculated above. The real and imaginary parts are calculated separately using the prescription

$$\frac{1}{r - i\epsilon} = P\Big(\frac{1}{r}\Big) + i\pi\delta(r). \tag{10}$$

Here $P\Big(\frac{1}{r}\Big)$ denotes the principal value. Note that for an electron state, $x = 0$ is an endpoint and the principal value prescription cannot be used. We take a small cutoff at $x = 0$.

The imaginary part of the amplitude when the electron helicity is not flipped is then given by

$$\begin{aligned} \mathrm{Im}[M_{++}](\zeta,\Delta^\perp) &= -i\pi e^2\Big[\int_0^\zeta dx\ F^{31}_{++}\ [\ \delta(x-\zeta)\ ] + \int_\zeta^1 dx\ F^{22}_{++}\ [\ \delta(x-\zeta)\ ]\ \Big] \\ &= -i\pi e^2\Big[F^{31}_{++}(x=\zeta,\Delta^\perp) + \ F^{22}_{++}(x=\zeta,\Delta^\perp)\ \Big]. \end{aligned} \tag{11}$$

A similar expression holds in the case when the electron helicity is flipped ($\mathrm{Im}[M_{+-}](\zeta,\Delta^\perp)$) in which F_{++} are replaced by F_{+-}. The helicity-flip DVCS amplitude is proportional to $(\Delta^1 - i\Delta^2)$ [14]. The results for these amplitudes will be presented with this kinematic factor removed. The imaginary part receives contributions at $x = \zeta$. The other regions of x contribute to the real part. It is to be emphasized that we are using the handbag approximation of the DVCS amplitude. Contributions from the Wilson lines are in general not zero, and they can give rise to new phase structures as seen in single-spin asymmetries [16].

The real part of the DVCS amplitude in our model is given by

$$\begin{aligned} \mathrm{Re}\ [M_{++}]\ (\zeta,\Delta^\perp) &= -e^2\int_\epsilon^{\zeta-\epsilon_1} dx\ F^{31}_{++}(x,\zeta,\Delta^\perp)\ \Big[\ \frac{1}{x}\ + P\Big(\ \frac{1}{x-\zeta}\ \Big)\Big] \\ &\quad -e^2\int_{\zeta+\epsilon_1}^{1-\epsilon} dx\ F^{22}_{++}(x,\zeta,\Delta^\perp)\Big[\ \frac{1}{x}\ + P\Big(\ \frac{1}{x-\zeta}\ \Big)\Big]. \end{aligned} \tag{12}$$

A similar expression holds for the helicity flip DVCS amplitude. The divergence at $x = \zeta$ gets canceled between the $2 \to 2$ and $3 \to 1$ contributions.

Calculation of the σ Fourier Transform

In order to obtain the DVCS amplitude in y^- space, we take a Fourier transform in ζ as,

$$A_{++}(\sigma, \Delta^\perp) = \frac{1}{2\pi} \int_{\epsilon_2}^{1-\epsilon_2} d\zeta \; e^{i\sigma\zeta} \; M_{++}(\zeta, \Delta^\perp),$$
$$A_{+-}(\sigma, \Delta^\perp) = \frac{1}{2\pi} \int_{\epsilon_2}^{1-\epsilon_2} d\zeta \; e^{i\sigma\zeta} \; M_{+-}(\zeta, \Delta^\perp), \tag{13}$$

where $\sigma = \frac{1}{2} P^+ y^-$ is the (boost invariant) longitudinal distance on the light-cone. We have imposed cutoffs at $\epsilon = \epsilon_1 = \epsilon_2/2 = 0.001$ for the numerical calculation. A detailed discussion of the cutoff scheme will be given in [14].

All Fourier transforms (FT) have been performed by numerically calculating the Fourier sine and cosine transforms and then calculating the resultant by squaring them, adding and taking the square root. In Fig. 1, we have shown the Fourier spectrum of the imaginary part of the DVCS amplitude with respect to ζ for $M = 0.5$ MeV, $m = 0.8$ MeV and $\lambda = 0.02$ MeV. (a) is the helicity non-flip and (b) is the helicity flip part of the amplitude. For all the plots, we have divided the amplitude by the normalization constant $e^4/(16\pi^3)$ and have taken $\Lambda = Q = 10$ MeV. The helicity non-flip amplitude depends on the scale Λ logarithmically and the scale dependence is suppressed in the helicity-flip part. As seen in Fig. 1 (a), for lower values of t, $Im[A_{++}]$ is almost flat, at higher values of $\mid t \mid$, the helicity non-flip amplitude displays a diffraction pattern in σ. Similar behavior is observed for other values of Q [14]. The peak becomes narrower and higher as $\mid t \mid$ increases. This can be explained because the moment with respect to x of the helicity non-flip GPDs gives the Dirac form factor of the electron which increases logarithmically with $\mid t \mid$. The number of minima increases with $\mid t \mid$ for fixed Q. In contrast, we see in Fig. 1 (b) that there is no diffraction pattern in the FT of the helicity-flip amplitude. This is due to the different behavior with respect to ζ of the respective amplitudes [14]. The peak of the $Im[A_{+-}]$ increases with $\mid t \mid$, attains a maximum for higher $\mid t \mid$, and then decreases. This is because the helicity-flip DVCS amplitude is related to the Pauli form factor of the electron which falls with $\mid t \mid$ for large $\mid t \mid$. The increasing behavior of the helicity flip amplitude $\gamma^* e^\uparrow (S_z^e = 1/2) \to \gamma e^\downarrow (S_z^e = -1/2)$ at small $\mid t \mid$ reflects the fact that one needs to transfer one unit of orbital angular momentum $\Delta L_z = \pm 1$ to the electron to conserve J_z. This assumes that the initial and final photon

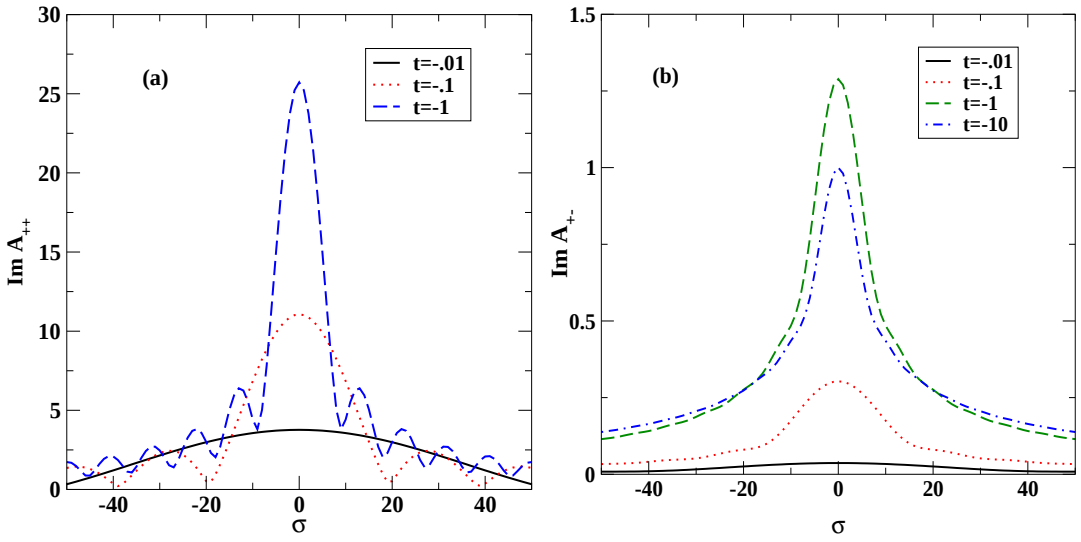

FIG. 1: Fourier spectrum of the imaginary part of the DVCS amplitude of an electron vs. σ for $M = 0.5$ MeV, $m = 0.8$ MeV, $\lambda = 0.02$ MeV, (a) when the electron helicity is not flipped; (b) when the helicity is flipped. The parameter t is in MeV^2.

have transverse polarization, which is what we use. A similar behavior is expected for $\gamma^* p^\uparrow(S_z^p = 1/2) \to \gamma p^\downarrow(S_z^p = -1/2)$ amplitude. The helicity-flip amplitude vanishes when t is zero.

In Fig. 2 we have plotted the Fourier Spectrum of the real part of the DVCS amplitude vs. σ for $M = 0.51$ MeV, $m = 0.5$ MeV and $\lambda = 0.02$ MeV. For the same $\mid t \mid$, the behavior is independent of Q when $\mid t \mid < m^2$. For each Q, the peak at $\sigma = 0$ is sharper and higher as $\mid t \mid$ increases, the number of minima within the same σ range also increases. As seen in Fig. 2, both the helicity flip and helicity non-flip parts show a diffraction pattern. The real part of the helicity flip amplitude in σ also decreases with t for higher t.

The DVCS amplitude for an electron-like state at one loop has potential singularities at $x = 0, 1$ and at $\zeta = 0$. As mentioned above, we have used cutoffs at these points. The helicity-flip part of the amplitude is not divergent at $x = 0, 1$ and is independent of the cutoffs but the real part of the helicity non-flip amplitude depends on these cutoffs. In the $2-$ and 3-body LFWFs, the bound-state mass squared M^2 appears in the denominator. Differentiation of the LFWFs with respect to M^2 increases the fall-off of the wavefunctions near the end points $x = 0, 1$ and mimics the hadronic wavefunctions. Differentiating once with respect to M^2 simulates a meson-like wavefunction and another differentiation simulates

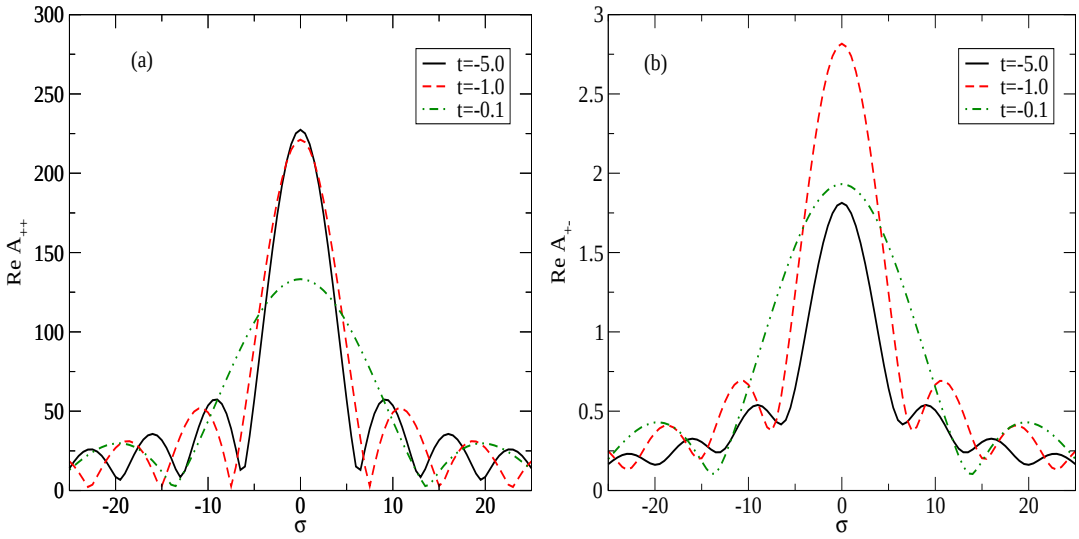

FIG. 2: Fourier spectrum of the real part of the DVCS amplitude of an electron vs. σ for $M = 0.51$ MeV, $m = 0.5$ MeV, $\lambda = 0.02$ MeV, (a) when the electron helicity is not flipped; (b) when the helicity is flipped. The parameter t is in MeV^2.

a proton wavefunction. Convolution of these wavefunctions in the same way as we have done for the dressed electron wavefunctions will simulate the corresponding DVCS amplitudes for bound state hadrons. One has to note that differentiation of the single particle wave function yields zero and thus there is no $3-1$ overlap contribution to the DVCS amplitude in this hadron model. It is to be noted that in recent holographic models from AdS/CFT as well [8] only valence LFWFs are constructed.

The equivalent but easier way is to differentiate the DVCS amplitude with respect to the initial and final state masses. Here we calculate the quantity $M_F^2 \frac{\partial}{\partial M_F^2} M_I^2 \frac{\partial}{\partial M_I^2} A_{ij}(M_I, M_F)$ where M_I, M_F are the initial and final bound state masses. For numerical computation, we use the discrete version of the differentiation

$$M^2 \frac{\partial A}{\partial M^2} = \bar{M}^2 \frac{A(M_1^2) - A(M_2^2)}{\delta M^2} \tag{14}$$

where $\bar{M}^2 = \frac{(M_1^2+M_2^2)}{2}$ and $\delta M^2 = (M_1^2 - M_2^2)$. We have taken $M_{I1}, M_{F1} = 150 + 1$, $M_{I2}, M_{F2} = 150 - 1$ MeV and fixed parameters $M = 150$ and $m = \lambda = 300$ MeV. In Figs. 3 and 4 we have shown the DVCS amplitude of the simulated hadron model, both as a function of ζ and after taking the FT in ζ. In Fig. 4 (c), we have plotted the structure function $F_2(x)$ in this model. The wave function is normalized to 1. There is another interesting aspect of this model. The $\gamma^* p \to \gamma p$ DVCS amplitude has both real [17] and imaginary parts [18]. If

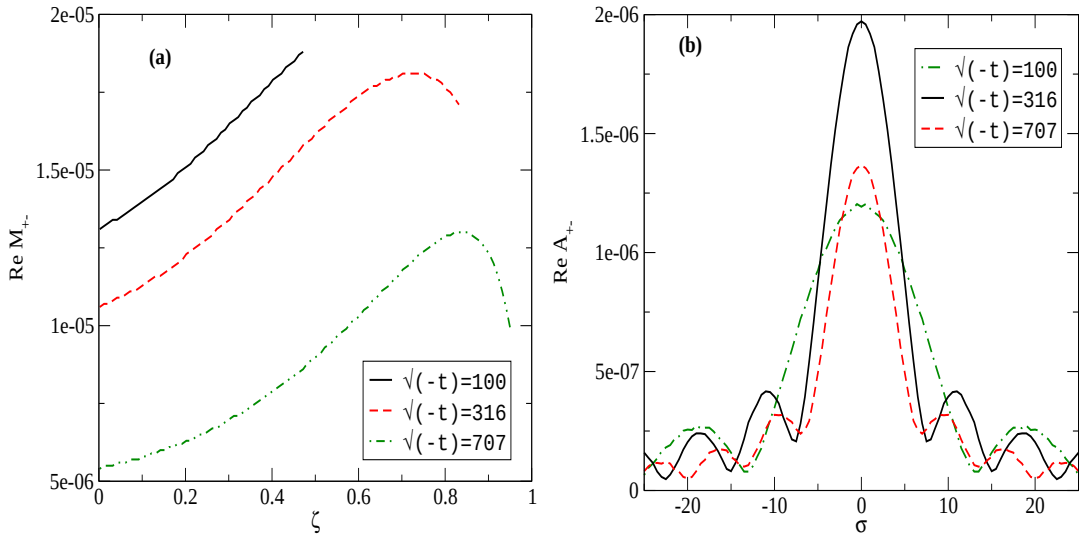

FIG. 3: Real part of the DVCS amplitude for the simulated meson-like bound state. The parameters are $M = 150, m = \lambda = 300$ MeV. (a) Helicity flip amplitude vs. ζ, (b) Fourier spectrum of the same vs. σ. The parameter t is in MeV^2.

we consider a dressed electron, the imaginary part from the pole at $x = \zeta$ survives because of the numerator $\frac{1}{x-\zeta}$ factor in the electron's LFWF. This numerator behavior reflects the spin-1 nature of the constituent boson. The $x - \zeta \to 0$ singularity is shielded when we differentiate the final state LFWFs with respect to M^2 and, as a result, the imaginary part of the amplitude vanishes in this model. We thus have constructed a model where the DVCS amplitude is purely real. It is interesting that the forward virtual Compton amplitude $\gamma^* p \to \gamma^* p$ (whose imaginary part gives the structure function) does not have this property. The pole at $x = \zeta$ is not shielded since the initial and final $n = 2$ LFWFs are functions of x. If instead we consider the differentiation with respect to the internal fermion mass m^2 rather than the bound state mass M^2, although it does not improve the wavefunction behavior at the endpoint $x = 0$, we can generate a model with both real and imaginary parts of the DVCS amplitudes.

From the plots, we propose an optics analog of the behavior of the DVCS amplitude in σ. In fact, the similarity of optics and quantum fields on the light cone was first explored long ago in [19, 20]. In the case of DVCS, we are effectively looking at the interference pattern between the plane wave of the initial virtual photon and the plane wave of the outgoing real photon. The final-state proton wavefunction is modified relative to the incident proton

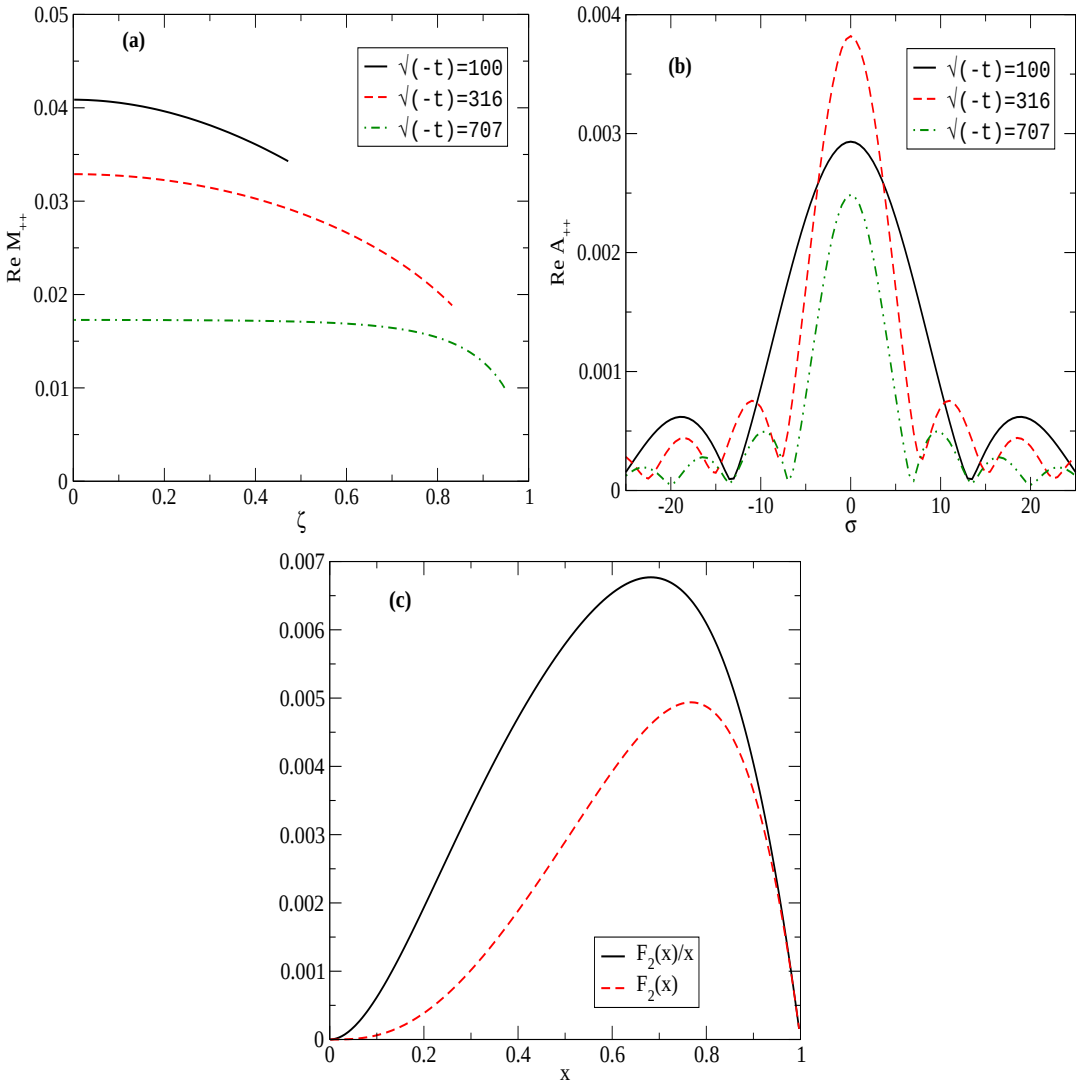

FIG. 4: Real part of the DVCS amplitude for the simulated meson-like bound state. The parameters are $M = 150, m = \lambda = 300$ MeV. (a) Helicity non-flip amplitude vs. ζ, (b) Fourier spectrum of the same vs. σ, (c) Structure function vs. x. The parameter t is in MeV^2.

wavefunction because of the momentum transferred to the quark in the hard Compton scattering. The change in quark momentum along the longitudinal direction ζ can be Fourier transformed to a boost-invariant distribution in the longitudinal light-front coordinate $\sigma = \frac{1}{2}y^- P^+$. In the case of the optical diffraction pattern obtained in a single-slit experiment, the size of the central maximum is inversely proportional to the width of the slit. Deeply virtual Compton scattering is analogous to the diffractive scattering of an electromagnetic wave in optics, where the diffractive pattern in σ reflects the size of the scattering center in units of the target's Compton scale.

We can study the diffraction pattern in σ as function of t or $\Delta_\perp^2$ in order to register the effect of a change in transverse momentum resulting from the Compton scattering. In the case of deeply virtual Compton scattering on the quantum fluctuations of a lepton target in QED, and also in the corresponding hadronic model, one sees that the diffractive patterns in σ sharpen and the positions of the first minima typically move in with increasing momentum transfer. Thus the invariant longitudinal size of the parton distribution becomes longer and the shape of the conjugate light-cone momentum distribution becomes narrower with increasing $\mid t \mid$. If one Fourier transforms the change in transverse momentum $\Delta_\perp$ to impact space $b_\perp$ [4, 5], then one would have the analog of a three-dimensional scattering center. In this sense, scattering photons in DVCS provides the complete Lorentz-invariant optics of a hadron.

This work was supported, in part, by the US Department of Energy grant Nos. DE-AC02-76SF00515, DE-FG02-97ER-41029, and DE-FG02-87ER40371 and at the University of California, Lawrence Livermore National Laboratory under contract No. W-7405-Eng-48. This work was also supported in part by the Indo-US Collaboration project jointly funded by the U.S. National Science Foundation (NSF) (INT0137066) and the Department of Science and Technology, India (DST/INT/US (NSF-RP075)/2001).

---

[1] S. J. Brodsky, M. Diehl, D. S. Hwang, Nucl. Phys. **B 596**, 99 (2001).

[2] M. Diehl, T. Feldmann, R. Jacob, P. Kroll, Nucl. Phys. **B 596**, 33 (2001), Erratum-ibid **605**, 647 (2001).

[3] X. D. Ji, Phys. Rev. Lett. **78**, 610 (1997) [arXiv:hep-ph/9603249].

[4] M. Burkardt, Int. Jour. Mod. Phys. **A 18**, 173 (2003).

[5] M. Burkardt, Phys. Rev. **D 62**, 071503 (2000), Erratum- ibid, **D 66**, 119903 (2002); J. P. Ralston and B. Pire, Phys. Rev. **D 66**, 111501 (2002).

[6] For a review, see S. J. Brodsky, H. C. Pauli and S. S. Pinsky, Phys. Rept. **301**, 299 (1998) [arXiv:hep-ph/9705477].

[7] K. Hornbostel, S. J. Brodsky and H. C. Pauli, Phys. Rev. **D 41**, 3814 (1990).

[8] S. J. Brodsky and G. F. de Teramond, arXiv:hep-ph/0602252.

[9] D. Chakrabarti, A. Harindranath and J. P. Vary, Phys. Rev. **D 71**, 125012 (2005); D.

Chakrabarti, A. Harindranath, L. Martinovic, G. B. Pivovarov and J. P. Vary, Phys. Lett. **B 617**, 92 (2005); D. Chakrabarti, A. Harindranath, L. Martinovic and J. P. Vary, Phys. Lett. **B 582**, 196 (2004).

[10] S. J. Brodsky and S. D. Drell, Phys. Rev. **D 22**, 2236 (1980).

[11] A. Harindranath, R. Kundu, A. Mukherjee, J. P. Vary, Phys. Rev. **D 58**, 114022 (1998); A. Harindranath and R. Kundu, Phys. Rev. **D 59**, 116013 (1999); A. Harindranath, R. Kundu, W. M. Zhang, Phys. Rev. **D 59**, 094013 (1999); A. Mukherjee and D. Chakrabarti, Phys. Lett. **B 506**, 283 (2001); A. Harindranath, A. Mukherjee, R. Ratabole, Phys. Lett. **B 476**, 471 (2000); Phys. Rev. **D 63**, 045006 (2001).

[12] D. Chakrabarti and A. Mukherjee, Phys. Rev. **D 71**, 014038 (2005); **D 72**, 034013 (2005).

[13] A. Mukherjee and M. Vanderhaeghen, Phys. Rev. **D 67**, 085020 (2003), Phys. Lett. **B 542**, 245 (2002).

[14] S. J. Brodsky, D. Chakrabarti, A. Harindranath, A. Mukherjee, J. P. Vary, in preparation.

[15] S. J. Brodsky, D. S. Hwang, B-Q. Ma, I. Schmidt, Nucl. Phys. **B 593**, 311 (2001).

[16] S. J. Brodsky, D. S. Hwang and I. Schmidt, Phys. Lett. **B 530**, 99 (2002) [arXiv:hep-ph/0201296].

[17] S. J. Brodsky, F. E. Close, J. F. Gunion, Phys Rev.**D 5**, 1384 (1972), **D 6**, 177 (1972), **D 8**, 3678 (1972).

[18] P. Kroll, M. Schurmann, P. A. Guichon, Nucl. Phys. **A 598**, 435 (1998); M. Diehl, T. Gousset, B. Pire, J. P. Ralston, Phys. Lett. **B 411**, 193 (1997); A. V. Belitsky, D. Muller, L. Niedermeier, A. Schafer, Phys. Lett. **B 474**, 163 (2000).

[19] E. C. G. Sudarshan, R. Simon and N. Mukunda, Phys. Rev. **A 28**, 2921 (1983); DOE-ER-03992-503.

[20] N. Mukunda, R. Simon and E. C. G. Sudarshan, Phys. Rev. **A 28**, 2933 (1983); DOE-ER-03992-504.